

This work was written as part of one of the author's official duties as an Employee of the United States Government and is therefore a work of the United States Government. In accordance with 17 U.S.C. 105, no copyright protection is available for such works under U.S. Law.

Public Domain Mark 1.0

<https://creativecommons.org/publicdomain/mark/1.0/>

Access to this work was provided by the University of Maryland, Baltimore County (UMBC) ScholarWorks@UMBC digital repository on the Maryland Shared Open Access (MD-SOAR) platform.

Please provide feedback

Please support the ScholarWorks@UMBC repository by emailing scholarworks-group@umbc.edu and telling us what having access to this work means to you and why it's important to you. Thank you.

Patterns of carbon monoxide in the middle atmosphere and effects of solar variability

Alexander Ruzmaikin^{a,*}, Jae N. Lee^b, Dong L. Wu^c

^a Jet Propulsion Laboratory, 4800 Oak Grove Dr., Pasadena, CA 91109, USA

^b Joint Center for Earth Systems Technology, University of Maryland, Baltimore County, 1000 Hilltop Circle, Baltimore, MD 21250, USA

^c NASA Goddard Space Flight Center, 8800 Greenbelt Rd, Greenbelt, MD 20771, USA

Available online 11 July 2013

Abstract

We determine the spatial-time patterns of zonally averaged carbon monoxide (CO) in the middle atmosphere by applying Principle Component Analysis to the CO data obtained from the Microwave Limb Sounder (MLS) measurements on the Aura satellite in 2004–2012. The first two principal components characterize more than 90% of the CO variability. Both principal components are localized in the low thermosphere near the mesopause. The first principal component is asymmetric relative to the poles. It has opposite signs in the Northern and Southern Hemisphere at mid to high latitudes and strongly oscillates with an annual periodicity. The second principal component has the same sign in both hemispheres and oscillates mainly with a semi-annual frequency. Both principal components are modulated by the 11-year solar cycle and display short-term variations. To test possible correlations of these variations with the short term solar ultraviolet (UV) variability we use the simultaneous measurements of the UV solar radiance from the Solar-Stellar Irradiance Comparison Experiment (SOLSTICE) on the Solar Radiation and Climate Experiment (SORCE) satellite to investigate the correlation between CO in the middle atmosphere and solar UV in 2004–2012. Using a wavelet coherence technique a weak, intermittent 27-day signal is detected in high-frequency parts of the CO principal components.

Published by Elsevier Ltd. on behalf of COSPAR.

Keywords: Middle atmosphere; Solar variability

1. Introduction

The primary source of carbon monoxide (CO) in the middle atmosphere is photolysis of carbon dioxide ($\text{CO}_2 + h\nu \rightarrow \text{CO} + \text{O}$). Most of the CO is produced in the upper mesosphere and thermosphere and transported down to the lower mesosphere and stratosphere near the polar regions (Solomon et al., 1985). The solar UV radiation absorbed in this reaction belongs mostly to the Schumann–Runge continuum 176–192.6 Å (Solomon et al., 1985; Allen et al., 1991/1992). Thus CO is expected to be sensitive to solar variability effects.

New accurate measurements of CO from the Microwave Limb Sounder (MLS) on the Aura satellite (Minschwaner

et al., 2010; Lee et al., 2011) along with simultaneous measurements of the solar irradiance from the Solar Radiation and Climate Experiment (SORCE) satellite (McClintock et al., 2000) open an opportunity to further investigate the global distribution of carbon monoxide in the middle atmosphere and trace the influence of solar variability on it. The Aura MLS and SORCE 2004–2012 data cover the recent solar minimum period between the cycles 23 and 24 and the beginning of the 24th solar cycle allowing useful insights on the solar-driven chemistry and dynamics of the middle atmosphere. Using MLS CO data for 2002–2012 Lee et al. (2013) showed that the solar-cycle variation dominates the long-term variability of the polar mesospheric CO concentration at high latitudes. The MLS CO time series was compared with the SORCE data and a significant, positive correlation up to 0.5 was found in the winter upper polar atmosphere suggesting that the interannual variability

* Corresponding author. Tel.: +1 8183933953.

E-mail address: Alexander.Ruzmaikin@jpl.nasa.gov (A. Ruzmaikin).

ity in mesospheric CO was induced by solar radiance changes.

Here we identify major patterns of spatial-time variability of CO in the middle atmosphere and investigate their relationship to solar variability. In addition to the solar cycle time scale we look at possible forcing of the middle atmospheric CO by the solar radiance on shorter time scales associated with the 27-day variability, which is caused by the solar rotation modulation of the UV radiation from the bright spots (faculae) on the solar surface. The 27-day variations in MLS stratospheric ozone and temperature have been investigated and compared with SORCE ultraviolet radiation (Ruzmaikin et al., 2007). Signatures of the 27-day solar rotation in mesospheric OH and H₂O were found in MLS data by Shapiro et al. (2012). To circumvent the problem of the time scale difference between solar variability and dynamical changes in CO we will investigate the correlation between the time variability of the global CO patterns and the solar UV.

2. Data and methods of data analysis

We use version 2.2 of the MLS CO data gridded separately for day and night. The data are assembled over pressure levels from the upper troposphere (316 hPa) to the top of the thermosphere (10^{-5} hPa). The typical single-profile precision of MLS V2.2 CO varies from 0.02 ppmv at 100 hPa, 0.2 ppmv at 1 hPa, to 11 ppmv at 0.002 hPa, with vertical resolution of 4, 3, and 9 km, respectively (Pumphrey et al., 2007). Here we focus on the range of levels

from 0.5 hPa (bottom of the mesosphere) to 0.001 hPa (low thermosphere). The MLS CO product at these heights has a systematic error of about 20% (see Table 2 in Pumphrey et al. (2007)). Because the errors increase with heights we do not use the data above 0.001 hPa. The daily CO fields are mapped onto a $4^\circ \times 8^\circ$ latitude-longitude grid. The Aura MLS data are provided for latitude bins between 84°S and 84°N . The data are processed for ascending (day) and descending (night) part of the satellite orbit. Here we show the results for the day-time data. The time period used in our study is from day 221, 2004 to day 265, 2012. There are 81 missing days in the MLS CO measurements. A large data gap occurred in between day 85–109 in 2011 with 23 missing days. To cover the gaps we interpolate the data between the missing days. For the interpolation we use the “inpaintn” algorithm (Garcia, 2010). The algorithm, based on the discrete cosine transform and a penalized least squares method, allows fast smoothing of data including data with large gaps that occurred in the MLS record. An iteratively weighted robust version of the algorithm takes care of missing and outlying values.

For solar UV we use the SORCE/SOLSTICE) data (McClintock et al., 2000) available at <http://lasp.colorado.edu/sorce/> from February 25, 2003 to May 2013. Here we use the measurements made by SOLSTICE B in the mid ultraviolet range 170–320 nm. The spectral radiance in the Schumann–Runge continuum is provided by the UV channels that measure the solar spectral irradiance in ultraviolet (UV) from 115 to 320 nm with a resolution of

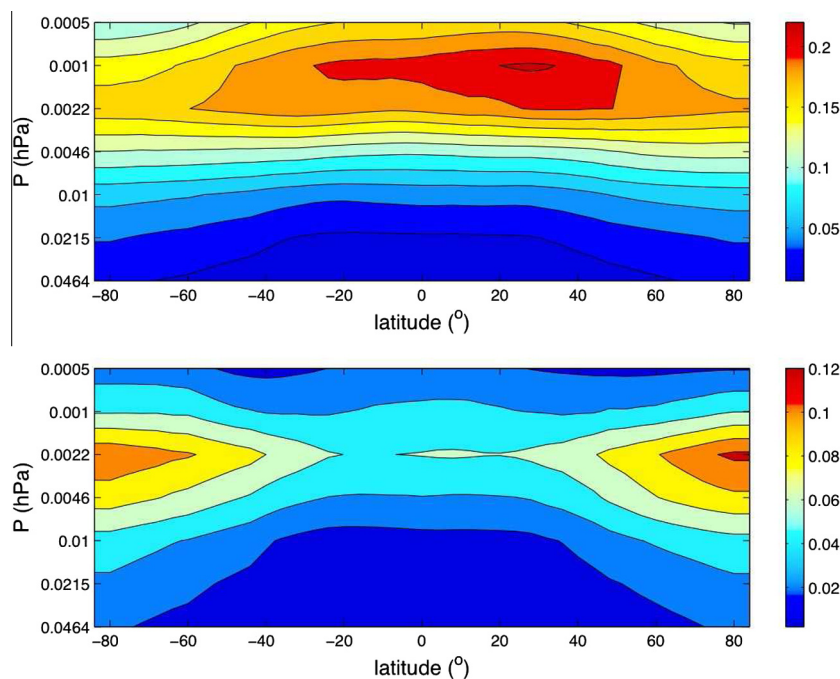


Fig. 1. The time mean of the zonally averaged CO (upper panel) and the standard deviation from this mean (lower panel). The colorbars show the values in filled contours in ppb. The standard deviation peaks near 0.002 hPa (in lower thermosphere at approximately 90 km). It is almost North–South symmetric and strongest in the mid and polar latitudes. The mean peaks above the 0.002 hPa height and is more concentrated around the equatorial region but not symmetrically with a slight bias toward the Northern latitudes.

0.1 nm and an absolute accuracy of better than 5%. We use the daily data for the same time period as the MLS data indicated above, interpolating between a small number of missing data days.

3. Spatial-time patterns of CO in the middle atmosphere

The MLS measurements provide a four-dimensional distribution of CO as a function of latitude, longitude, height, and time. Here we consider the zonally averaged distribution. The time averaged (mean) of this distribution and its standard deviation are shown in Fig. 1. To remove a potential seasonal bias we calculated the mean and standard deviation for exactly 8 years (from day 265 in 2004 to day 265 in 2012) although the inclusion of the whole data set does not substantially affects these values. We note a slight North–South asymmetry of the mean. The standard deviation is North–South symmetric and peaks at 0.002 hPa in accord with the variations characterized below by the principal component modes.

We reduce the dimension of the data set by identifying the correlated patterns of the zonally-averaged CO. The availability of the global data coverage allows us to apply

the methods of pattern identification that take into account the space–time correlations between the grid points. We apply the well-known Principal Component Analysis [PCA, c.f. Preisendorfer, 1988] to identify the major spatial patterns of the CO and their time variability in the middle atmosphere. The major patterns are well represented by the first two Empirical Orthogonal Functions (EOFs) as functions of latitude and height and the corresponding principal components (PCs) as functions of time, see Fig. 2. These two principal components are not affected by data noise that populates the high-order principal components. The first two EOFs account for 58.9% and 36.1% of variability correspondingly. The remaining principal components contribute 2.4%, 1.3%, 0.8%, etc in the order of their eigenvalues and are not considered here. The total CO concentration can be restored as its mean value and the sum of all principal components proportional to the products $PC \times EOF$. In our estimates and figures we include the variability weights (listed above in %) into the definition of PCs.

The first EOF has the form of a North–South dipole which oscillates reflecting strong seasonal variation of the CO distribution. It has a narrow distribution in height

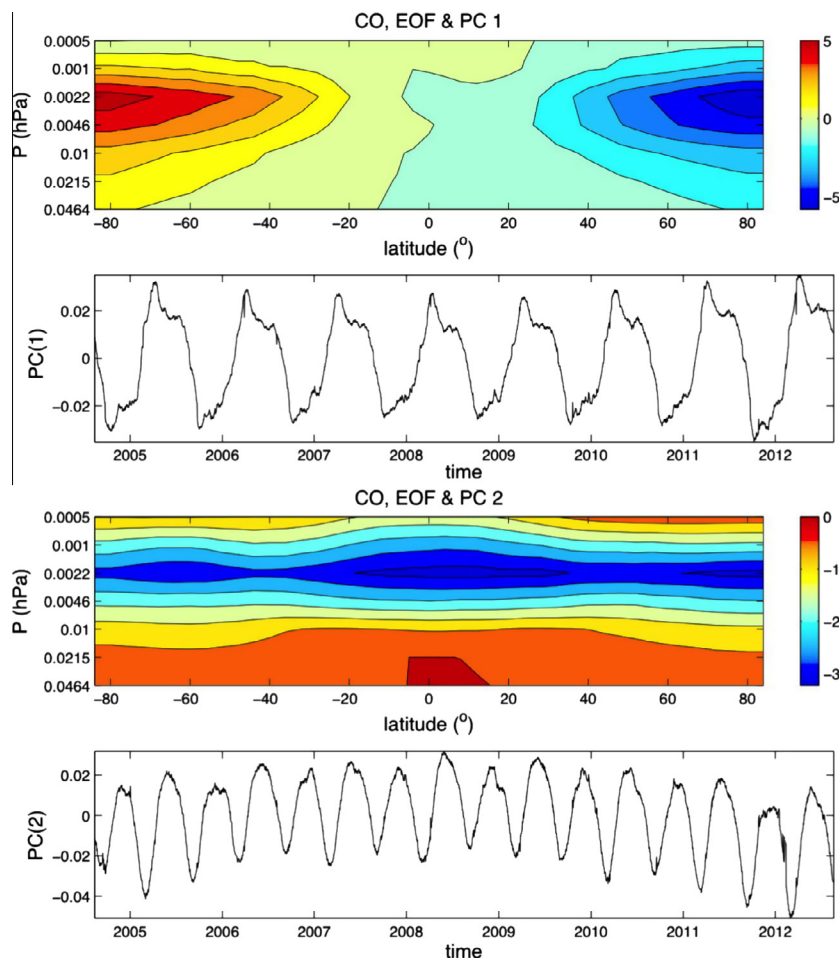


Fig. 2. Two major PCA modes of zonally-averaged CO. The first and third panels show the spatial distribution of the modes (EOFs), the second and fourth panel show the principal components, i.e. time dependence associated with the EOFs. The colorbars for EOFs are displayed in ppb units. Both modes peak near 0.002 hPa. The colors reverse with the annual periodicity for the first EOF and with the semi-annual periodicity for the second EOF.

peaking at 0.0022 hPa, i.e. in the low thermosphere near the mesopause, at about 90 km. The fact that the first EOF has opposite signs in the Northern and Southern Hemisphere indicates that when CO reaches maximum in the North it is minimal in the South with the reverse of sign after a half year. The second EOF has the same sign in both hemispheres and has a maximum in the equatorial region and at high northern latitudes. The corresponding PC oscillates mainly with a semi-annual frequency. Both PCs are clearly modulated by the 11-year solar cycle.

4. Search for 27-day solar forcing of CO

The question addressed in this section is whether the high-frequency variations superimposed on the annual and semi-annual oscillations of the principal components result from the forcing by short-term solar variability. The short-term variability of the UV radiation arises because the bright spots on the surface of the Sun (faculae) appear and disappear from the view due to the 27-day solar rotation. It is known that the 27-day solar UV signal is not persistent, it is strong at solar maxima and almost undetectable near solar minima, (cf. Shapiro et al., 2012). The situation is worsened by the fact that the solar activity in

the time period under consideration was substantially suppressed near the current minimum of the Centennial Gleissberg Cycle (Feynman and Ruzmaikin, 2012).

Fig. 3 shows the time series of the UV signal in the Schumann–Runge band detected by the SORCE (upper panel). The direct Fourier spectrum of this signal has 27-day and 13.5-day peaks (second panel). The problem with the spectral approach is that the standard Fourier spectrum is taken over the entire time series and thus smears the signal that actually appears over intermittent time intervals. To overcome this problem we use the wavelet decomposition of the time series into a time-frequency domain (third panel). We see that the contribution to the 27-day integral Fourier spectral mode comes mainly from the beginning and the end of the time series i.e. from time intervals when the Sun was at maxima of its activity.

The direct Fourier spectrum of the CO PCs does not show significant 27-day and 13.5-day peaks. To see whether there is a 27-day mode in the CO we first filtered out all spectral modes with frequency lower than 54-days using the wavelet filtering code ‘wavedec’ (available for example in Matlab library). The filtered PC 1 and PC 2 are shown in the upper panels in Figs. 4, 5. Their wavelet spectra (second panels in Figs. 4, 5) show an intermittent

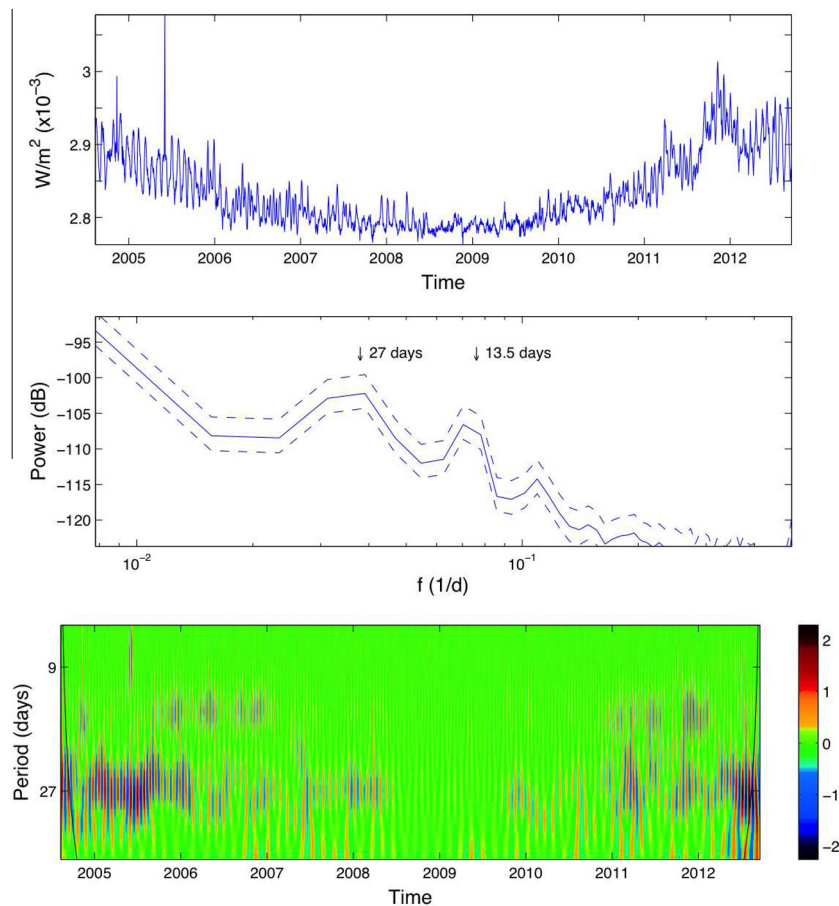


Fig. 3. Fourier and wavelet spectra of solar UV in the Schumann–Runge continuum (second and third panels). The wavelet power shown in color is normalized by the factor 10^{-4} . The data (upper panel) are from SORCE measurements in 2004–2012. The 13.5-day signal appears differently in time compare with the 27-day signal. Thus the 13.5-day signal peaks in 2006 and 2011, while the 27-day signal peaks in 2005 and 2012.

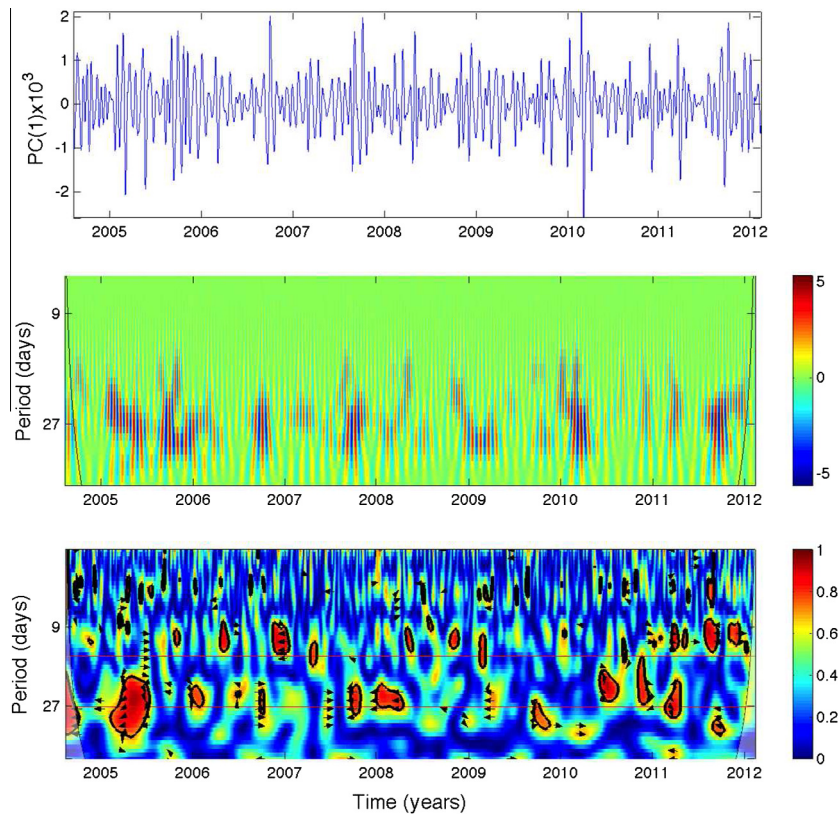


Fig. 4. Time series of the filtered first principal component of MLS CO at the short time scale range (1–54 days) in 2004–2012 (upper panel). Wavelet spectrum of the time series shown above (middle panel). The time dependent correlation of the first CO mode and solar UV displayed with the wavelet coherence technique (lower panel). The color indicates the level of correlation in the range 0:1, arrows show the sign of correlation.

27-day signal. The 27-day signal in the first EOF (Fig. 4, second panel) is mainly seen in the northern latitude summer (as well as in spring and fall) time but in the second EOF (Fig. 5, second panel) it is seen mainly in the northern latitude winter time although there is a seasonal dependence in the second EOF.

Due to the intermittent character of the signal we track the time dependent correlations between the solar UV time series and the CO PCs time series using the wavelet coherence technique designed by Grinsted et al. (2004). The technique expands the estimate of traditional correlation coefficient to a correlation coefficient in time-frequency domain allowing us to localize parts of two time series with potential correlations. We see that the correlations between the UV and CO on the 27-day and 13.5-day time scale appear intermittently (third panels in Figs. 4,5).

5. Conclusions and discussion

We find that the major spatial-time structures (principal components) of the CO variability are localized in the 0.01–0.001 hPa range of the middle atmosphere (upper mesosphere to low thermosphere) with maxima in the low thermosphere at 0.002 hPa (near the mesopause, at about 90 km). The first two principal components account for more than 90% of CO variability. The modes vary annually and semi-annually correspondingly with superimposed 11-

year modulation and exhibit small amplitude high-frequency oscillations.

We presented the results of our study using the day-time CO data. Principal component analyses of the night-time data show similar patterns. Since CO is affected by the Sun photochemically, sunlight is obviously needed. To explain why the use of the night data results in the same structures we need to look at the lifetime of CO in the parts of the middle atmosphere under consideration. The photochemical lifetime of CO (due to its destruction by the three-body recombination with atomic oxygen and by the collision with OH) and transport time of CO in the middle atmosphere strongly vary with height (Solomon et al., 1985). The photochemical time is shorter than the transport time in the stratosphere and low mesosphere but becomes comparable to the transport time at about 75 km, where both times are about a month. At higher altitudes, and in particular in the low thermosphere, the CO photochemical lifetime is large, exceeding a year. Because the lifetime of CO there is much longer than a day the spatial-time structures determined from the day and night data are similar.

The principal components have strongly outlined spatial and time structures. Their narrow distribution in height can possibly be explained by the facts that the three-body recombination (thermospheric loss) is mostly effective above 100 km and the loss due to collisions with OH is

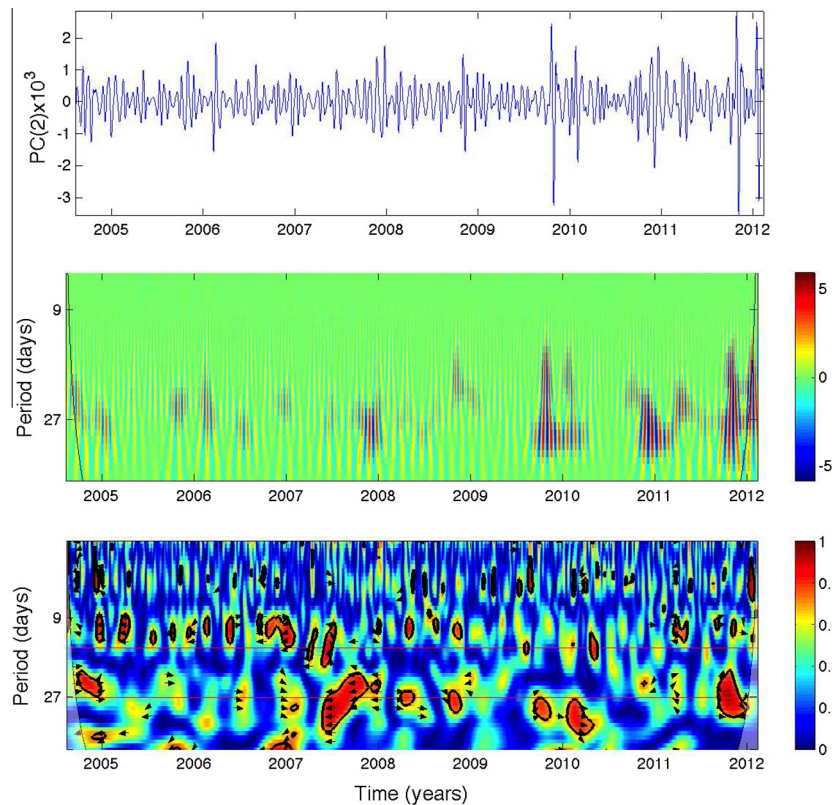


Fig. 5. The same as Fig. 3 for the second principal component.

mostly effective in the stratosphere and low mesosphere. The first EOF is asymmetric relative to the poles, it has a form of North–South dipole distributed with the opposite signs at mid and high latitudes. This latitudinal structure may be formed by the winter descent of CO in the Northern Hemisphere, which brings the high CO concentration downward, while ascent in the Southern Hemisphere brings the low CO concentration upward. The second EOF has the same sign in both hemispheres and slightly maximizes over the tropical latitudes. A dynamical explanation of the latitudinal structure of the second EOF remains to be found. A reviewer of this paper suggested a photochemical explanation due to the seasonally-varying source of CO produce by the photolysis of CO₂. It appears that the minima of PC2 are at the equinoxes (when the Sun is over the equator) and the maxima at the solstices (when the Sun is at maximum declination). The EOF2 has a minimum in the tropics, which would mean that the maximum of CO in the tropics (PC2 × EOF2) occurs at the equinoxes.

Note that strictly speaking, we can not directly interpret the EOFs in terms of descending/ascending transport of CO since that type of interpretation is not offered by the principal component analysis that only takes care of spatial correlations across the whole domain at each time.

The annual variation of the CO can easily be understood since during the solstices, the CO is transported by the single cell circulation with rising motion in the summer hemisphere and sinking motion in the winter hemisphere. This circulation pattern is generally driven by small scale gravity

waves (Andrews et al., 1987). These waves occur during all seasons and at all latitudes in the mesosphere. The satellite wind observations indicate that diurnal tides and amplitudes of meridional and zonal winds are significantly larger near equinox than those near solstice, thereby displaying strong semiannual variations (Burrage et al., 1996). For discussion of causes of these tidal variations, involving gravity and Kelvin waves see Garcia et al. (1997). The time dependence and spatial structure of the CO second principal component could be closely related to the wind variation and its structure in the high mesosphere – low thermosphere.

Since the solar UV flux is critical to the CO photolysis, the measurements of spectral solar radiance are valuable for understanding of atmospheric responses to solar spectral forcing. Although the middle atmospheric CO mostly changes on annual and semi-annual time scales there is evidence of influence of solar variability on the 11-year time scale. The effects on the short 27-day time scale appear to be weak and intermittent probably due to the intermittent character of the solar UV forcing. The cause for the weak solar affect on the short time scale is due to the fact that to date the MLS measurements have been carried out in the time period 2003–2012, which covers the declining phase of the solar cycle 23, the deep 23/24 cycle minimum, and the rising part of the weak cycle 24. A complete solar cycle will be very useful for estimating the amplitude of 27-day variations in CO over the 11-year solar cycle and will contribute to understanding the sun-climate connections; in

particularly in understanding how the spectral changes of the solar radiative output play a role in these connections.

Acknowledgments

We thank two reviewers for helpful critical comments. This work was supported in part by the Jet Propulsion Laboratory of the California Institute of Technology, under a contract with the National Aeronautics and Space Administration. We acknowledge the NASA LWS grant on observational study of solar variability impacts on the troposphere, stratosphere and mesosphere.

References

- Allen, D.R., Stanford, J.L., Lopez-Valverde, M.A., Nakamura, N., Lary, D.J., Douglass, A.R., Cerniglia, M.C., Remdios, J.J., Taylor, F.W. Observations of middle atmosphere CO from the UARS ISAMS during the early northern winter 1991/1992. *J. Atmos. Sci.* 56, 563–583, 1991/1992.
- Andrews, D.G., Holton, J.R., Leovy, C.B. *Middle Atmosphere Dynamics*. Academic, Orlando, Fla, p. 489, 1987.
- Burrage, M.D., Vincent, R.A., Mayr, H.G., Skinner, W.R., Arnold, N.F., Hays, P.B. Long term variability in the equatorial mesosphere and lower thermosphere zonal winds. *J. Geophys. Res.* 101, 12847–12854, 1996.
- Feynman, J., Ruzmaikin, A. The Centennial Gleissberg Cycle in space weather in Space Weather: The Space Radiation Environment. AIP Conf. Proc. 1500, 44–49, <http://dx.doi.org/10.1063/1.4768743>, 2012.
- Garcia, D. Robust smoothing of gridded data in one and higher dimensions with missing values. *Comput. Stat. Data Anal.* 54, 1167–1178, 2010.
- Garcia, R.R., Dunkerton, T.J., Lieberman, R.S., Vincent, R.A. Climatology of the semi-annual oscillation of the tropical middle atmosphere. *J. Geophys. Res.* 102, 26019–26032, 1997.
- Grinsted, A., Moore, J.C., Jevrejeva, S. Application of the cross wavelet transform and wavelet coherence to geophysical time series. *Nonlinear Process. Geophys.* 11, 561–566, 2004.
- Lee, J.N., Wu, D.L., Manney, G.L., Schwartz, M.J., Lambert, A., Livesey, N.J., Minschwaner, K.R., Pumphrey, H.C., Read, W.G. Aura microwave limb sounder observations of the polar middle atmosphere: dynamics and transport of CO and H₂O. *J. Geophys. Res.* 116, D05110, <http://dx.doi.org/10.1029/2010JD014608>, 2011.
- Lee, J.N., Wu, D.L., Ruzmaikin, A. Interannual variations of MLS carbon monoxide induced by solar cycle. *Phys.* 102, 99–104, 2013.
- McClintock, W.E., Rottman, G.J., Woods, T.N. Solar stellar irradiance comparison experiment II (SOLSTICE II) for the NASA earth observing system's solar radiation and climate experiment mission. *SPIE Proc.* 4135, 225–234, 2000.
- Minschwaner, K., Manney, G.L., Livesey, N.J., Pumphrey, H.C., Pickett, H.M., Froidevaux, L., Lambert, A., Schwartz, M.J., Bernath, P.F., Walker, K.A., Boone, C.D. The photochemistry of carbon monoxide in the stratosphere and mesosphere evaluated from observations by the microwave limb sounder on the aura satellite. *J. Geophys. Res.* 115, D13303, <http://dx.doi.org/10.1029/2009JD012654>, 2010.
- Preisendorfer, R.W. *Principal Component Analyses in Meteorology and Oceanography*. Elsevier Pbls, 1988.
- Pumphrey, H.C. et al. Validation of middle-atmosphere carbon monoxide retrievals from the microwave limb sounder on aura. *J. Geophys. Res.* 112, D24S38, <http://dx.doi.org/10.1029/2007JD008723>, 2007.
- Ruzmaikin, A., Santee, M.L., Schwartz, M.J., Froidevaux, L., Pickett, H. The 27-day variations in stratospheric ozone and temperature: new MLS data. *Geophys. Res. Lett.* 34, L02819, <http://dx.doi.org/10.1029/2006GL028419>, 2007.
- Shapiro, V.E., Rozanov, E., Shapiro, A.I., Wang, S., Egorova, T., Schmutz, W., Peter, Th. Signature of the 27-day solar rotation cycle in mesospheric OH and H₂O observed by the aura microwave limb sounder. *Atmos. Chem. Phys.* 12, 3181–3188, 2012.
- Solomon, S., Garcia, R.R., Olivero, J.J., Belvilacqua, R.M., Schwartz, P.P., Clancy, R.T., Muhleman, D.O. The photochemistry and transport of carbon monoxide in the middle atmosphere. *J. Atmos. Sci.* 42, 1072–1083, 1985.